The high resolution crystal structure of rat liver AKR7A1: Understanding the substrate specificites of the AKR7 family

ARTICLE *in* CHEMICO-BIOLOGICAL INTERACTIONS · MARCH 2003

Impact Factor: 2.58 · DOI: 10.1016/S0009-2797(02)00186-2 · Source: PubMed

4 AUTHORS, INCLUDING:

Elizabeth Ellis
University of Strathclyde
70 PUBLICATIONS **1,445** CITATIONS
SEE PROFILE

Adrian J Lapthorn
University of Glasgow
57 PUBLICATIONS **2,477** CITATIONS
SEE PROFILE

Available online at www.sciencedirect.com
SCIENCE DIRECT®
Chemico-Biological Interactions 143–144 (2003) 289–297
Chemico-Biological Interactions
www.elsevier.com/locate/chembioint

The high resolution crystal structure of rat liver AKR7A1: understanding the substrate specificites of the AKR7 family

Evelin Kozma [a], Elaine Brown [a], Elizabeth M. Ellis [b], Adrian J. Lapthorn [a,*]

[a] Department of Chemistry, University of Glasgow, Glasgow G12 8QQ, UK
[b] Departments of Bioscience and Pharmaceutical Sciences, University of Strathclyde, Glasgow, UK

Abstract

The structure of the rat liver aflatoxin dialdehyde reductase (AKR7A1) has been solved to 1.38 Å resolution. The crystal structure reveals details of the ternary complex as one subunit of the dimer contains NADP+ and the inhibitor citrate. The underlying catalytic mechanism appears similar to other aldo–keto reductases (AKR), whilst the substrate-binding pocket contains several positively charged amino acids (Arg-231 and Arg-327) which distinguishes it from the well characterised AKR1 family of enzymes. These differences account for the substrate specificity for 4-carbon acid-aldehydes such as succinic semialdehyde (SSA) and 2-carboxybenzaldehyde, as well as for the idiosyncratic substrate aflatoxin B1 dialdehyde of this subfamily of enzymes. The AKR7 enzymes seem to be subdivided into two subgroups based on their sequence and kinetic properties. Modelling of the rat AKR7A4 highlights important structural differences localised within the active site of the two isoenzymes.

Keywords: AKR7; Molecular modeling; Substrate specificity; Crystal structure

1. Introduction

The aldo–keto reductases (AKR) are a superfamily of enzymes [1] present in a wide range of organisms, from bacteria to man. The enzymes have been divided into fourteen families (AKR1 to AKR14) [2,3] (http://www.med.upenn.edu/akr/), membership to a particular family is dependent on greater than 40% amino acid identity. These families are then grouped into subfamilies if the enzymes share greater than 60% amino acid identity. They share a common architecture of a $(\alpha/\beta)_8$ barrel structure which was first demonstrated for human aldose reductase (AKR1B1) [4,5]. Despite their overall structural similarity, these enzymes show considerable diversity in terms of substrate specificity, acting on numerous aliphatic and aromatic aldehydes and ketones, including sugars, steroids and xenobiotics. Representative crystal structures have been determined for the AKR1A family, porcine aldehyde reductase (AKR1A1) [6]; AKR1B family, human

* Corresponding author
E-mail address: andrian@pop.chem.gla.ac.uk (A.J. Lapthorn).

0009-2797/02/$ - see front matter
PII: S0009-2797(02)00186-2

aldose reductase (AKR1B1) [4], AKR1C family, rat liver 3-α hydroxysteroid dehydrogenase (AKR1C1) [7], AKR3A family, yeast GCY1 (AKR3A1) [8], AKR5C family, bacterial 2,5-diketo-D-gluconic acid reductase (AKR5C) [9], and AKR6 family, rat K^+ Channel β subunit (AKR6A2) [10]. A comparison of the sequences of the various AKR enzymes that currently make up the superfamily shows that they are split into two branches: AKR families 1–5 cluster as one branch, the remaining families cluster as the other branch [3]. Almost all mammalian AKRs belong to the first branch of the superfamily, the exceptions are the K^+ Channel β subunit (AKR6) which has no apparent enzyme activity and the aflatoxin dialdehyde reductases (AKR7).

Rat liver aflatoxin dialdehyde reductase (AFAR; AKR7A1) was first identified as a cytosolic NAD(P)$^+$-dependent reductase capable of reducing the dialdehyde phenolate metabolite of aflatoxin B_1 [11,12]. Cloning and sequencing of the gene encoding this enzyme [13] identified it as a belonging to the AKR superfamily and the founder member of the AKR7 family. AKR7A1 is unusual amongst AKR in that it is able to reduce aflatoxin B_1 dialdehyde, it can however, also reduce a wide range of aldehydes and diketones, and has particularly high affinity for succinic semialdehyde (SSA) and 2-carboxy-benzaldehyde (2-CBA) and 9,10-phenanthrenequinone [14,15]. Four other members of the AKR7 family have now been identified: these are human AKR7A2 [16], human AKR7A3 [17], rat AKR7A4 [15] and more recently mouse AKR7A5 [18]. Rat AKR7A4, human AKR7A2 and mouse AKR7A5 form a distinct grouping based on their sequence similarity that may reflect related functions of these enzymes, and suggests a functional difference from the rat AKR7A1 which appears to form a different sub-grouping (Hinshelwood et al., this issue). Of particular interest is the finding that human AKR7A2 functions as a SSA reductase in brain, and may, therefore, play a role in the production of γ-hydroxybutyrate (GHB) [15,19]. We have recently determined the structure of AKR7A1 [20], the details of which are reviewed here. In addition we use the crystal structure of the AKR7A1 ternary complex to model the related second rat enzyme AKR7A4. Differences in the primary sequence can be put into a three dimensional context and thereby related to the substrate specificity and possible function of the AKR7A4 enzyme.

2. Methods

2.1. Crystal structure determination

The structure of AKR7A1 was solved using single X-ray crystal analysis as described previously [20]. Briefly, crystals of AKR7A1 were grown over several days using the sitting drop vapour diffusion method with 20% polyethylene glycol 8000, 0.2 M lithium sulphate, 0.1 M sodium citrate pH 5.6 as the precipitant solution. An 85% complete X-ray data set was collected to 1.38 Å resolution on crystals flash frozen at 100 K at the European Molecular Biology Laboratory BW7B, DESY, Hamburg. The crystals were monoclinic C2 with unit cell dimensions $a = 125.54$ Å, $b = 64.68$ Å, $c = 112.84$ Å and $\beta = 91.0^\circ$ with two molecules in the asymmetric unit. The structure was solved by molecular replacement methods using the structure of AKR6A2 [21] as a search model. Although this solution was a poor starting model, the high resolution data allowed the use of automated structure building using the program ARP/WARP [22]. In this way 507 residues were built, and assembled into A (85% complete) and B (75% complete) chains of AKR7A1. Five iterations of refinement using REFMAC5 [23] and manual rebuilding using QUANTA (Accelyrs Inc.) allowed the completion of the structures and the addition of molecules of $NADP^+$, citrate and glycerol. The application of individual anisotropic temperature factors in the final stages of refinement, resulted in a model with the final R_{work} of 15.7% and R_{free} of 17.8%.

2.2. Modelling of AKR7A4

Modelling of AKR7A4 was carried out using the web based utility SWISSMODEL (http://www.expasy.ch/swissmod/SWISS-MODEL.html) using the structure of the ternary complex of

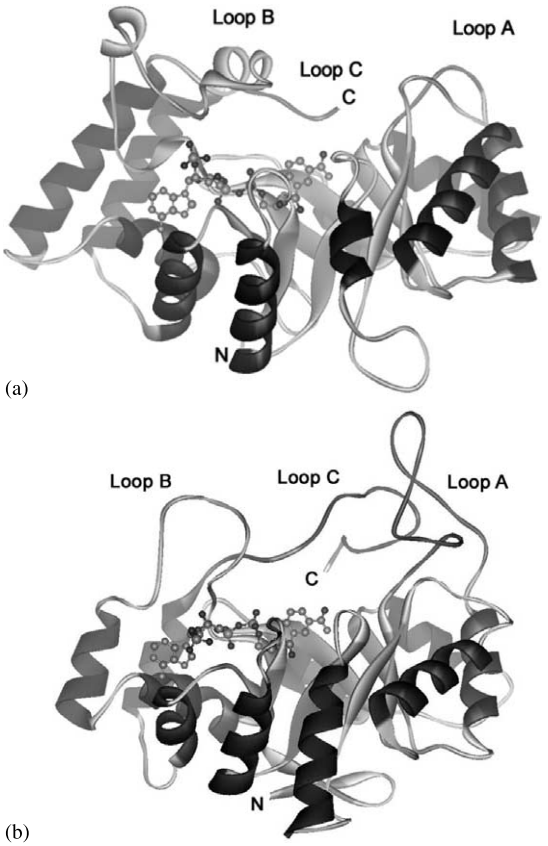

Fig. 1. Ribbon diagrams based on (a) the ternary complex of rat aflatoxin reductase AKR7A1 (b) the ternary complex of human aldose reductase illustrate the overall fold of these two enzymes. The Loops A, B and C are labelled highlighting their different size and structure. The cofactor $NADP^+$ is shown as ball and stick representation and the diagram was produced using WEBLAB viewer (Accelrys Inc.)

AKR7A1 as a template. Due to the high sequence identity between the two proteins (79.3%) it was hoped that a structural model would identify accurately differences between the two enzymes. The initial model obtained from SWISSMODEL was analysed using QUANTA (Accelyrs Inc.) to check manually for steric clashes and that the most chemically sensible orientation for each modified residues was used. A number of sidechains were moved to lower energy orientations, these were selected using the sidechain rotamer library within the module XBUILD of QUANTA. After this no further optimisation or energy minimisations of the model were performed.

Fig. 2. A ribbon representation of the AKR7A1 dimer with the cofactor shown in ball and stick in chain A (ternary complex) and absent in chain B (apo enzyme). The N and C termini of both chains are labelled but the break in chain B between residue 208 and 232 of Loop B is not.

3. Results and discussion

3.1. Comparative features of AKR7A1

The AKR7A1 structure contains two nonidentical molecules in the asymmetric unit, one the apo-enzyme and the other the ternary complex (enzyme–$NADP^+$–inhibitor), the inhibitor being the tricarboxylic acid citrate from the precipitant solution. A comparison of the AKR7A1 ternary complex with the equivalent complex of AKR1B1, aldose reductase highlights a number of the major structural differences (Fig. 1). For example, the base of the β-barrel is normally covered by two short β-strands formed by the N-terminus but in AKR7A1 these are absent. The second α-helix in the barrel is much shorter than usual with a triple Leu-Gly repeat ending the helix and forming an extended loop structure with the leucines buried in the hydrophobic core.

Loop A, a 23 amino acid loop present in all AKR1s (Fig. 1b) is effectively absent in AKR7A1, changing the shape of the active site cavity. A seven residue loop between β3 and α3 contributes some residues (Met-77 and Phe-78) to the space normally occupied by Loop A residues in AKR1 enzymes. Loop B of AKR7A1, which forms a large lid over the active site (Fig. 1a), is the longest such loop (35 residues compared with 12 for AKR1B1) of any known AKR. From Loop B Arg-204, Tyr-204, Pro-215, Ser-217 and Arg-218

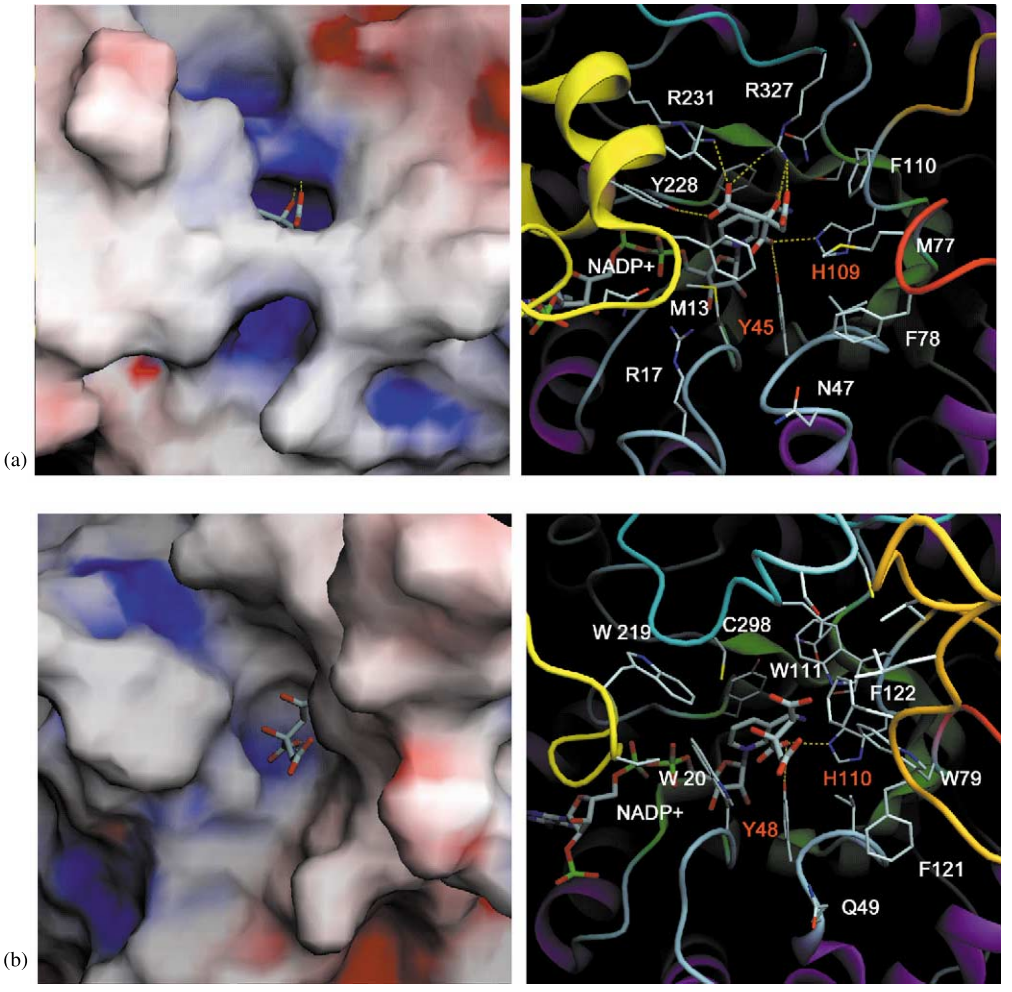

Fig. 3. Detailed views of the active site of (a) AKR7A1 and (b) AKR1B1, both with citrate bound in the active site. The left-hand frame is a surface representation of enzyme coloured according to electrostatic potential with blue representing positive potential and red negative potential. The right-hand frame is a detail of the same view with β-strands are coloured green, α-helices purple, Loop A orange, Loop B yellow, Loop C cyan and a short loop between strand β3 and α3 is coloured red. Residues are coloured according to atom type. The citrate and $NADP^+$ cofactor are both shown as thicker sticks than the protein side chains. The catalytic tyrosine and histidine are labelled in red for clarity. The diagram was produced using DINO (http://www.biozentrum.unibas.ch/ ~ xray/dino/) the surface and electrostatic potential calculations performed using GRASP [26].

are involved in cofactor binding and occupy the same relative positions as residues from the AKR6A2 structure. The cofactor makes numerous contacts with protein as in other AKRs; the nicotinamide ring is bound in the middle of the α/β barrel at the active site, the pyrophosphate group between the β-strands β7 and β8, and the adenine mono-phosphate moiety between helices α7, α8 and Loop B.

Helices H1 and H2 in most AKRs are eight to ten residues long, however, in AKR7A1 these are extended and are between 12 and 19 residues long. This has the effect of reducing the length of the C-terminal loop to five residues which contrasts to the 23 residues for AKR1B1. The last residue of the C-terminus, Arg 327 is positioned into the active site, thus loop C plays a role in the active site of AKR7A1 as in all active AKR enzymes.

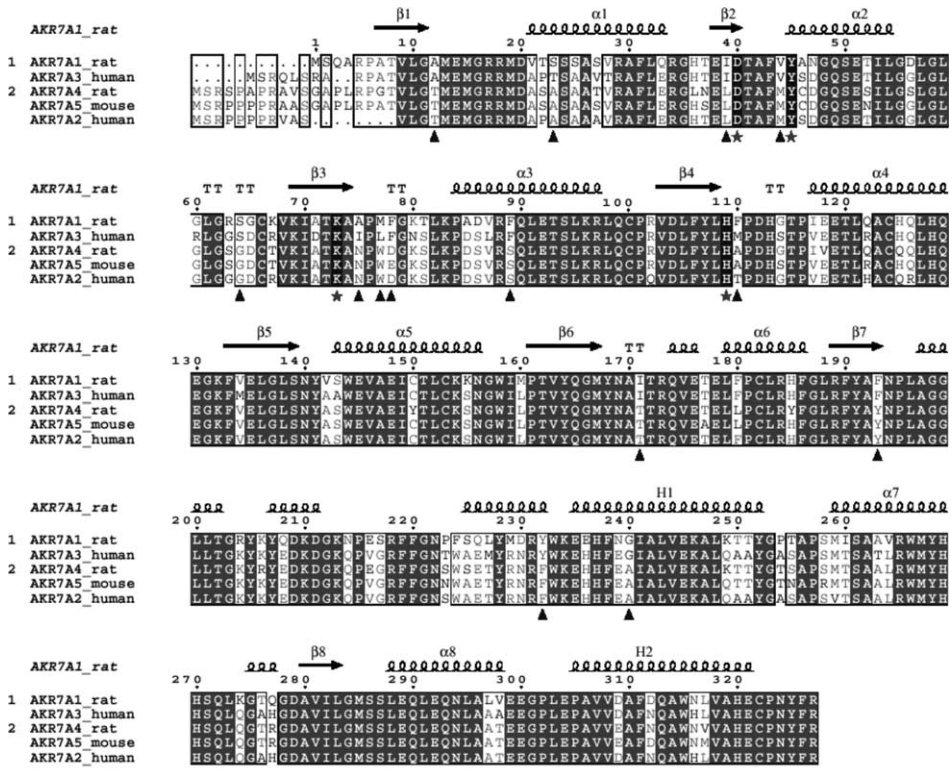

Fig. 4. (a) A sequence alignment of the known members of the AKR7 family of enzymes, separated into two sub groups and compared with the secondary structure of AKR7A1. α-helices and β-strands are represented as helices and arrows, respectively, and β-turns are labelled with TT. The catalytic tetrad is marked with a * while key residues which differ between the two AKR7 sub groups are marked with ▲. The diagram was produced using ESPRIPT [27]. (b) A tube representation of the AKR7A1 structure with the position of the residues that differ between the two AKR7 sub groups coloured black. The marked residues that fall within the active site are labelled. The position of the catalytic tyrosine and histidine are shown in stick representation, as is the position of the co-factor $NADP^+$. The diagram was composed in WEBLAB viewer (Accelrys Inc.)

3.2. Dimerisation

Most AKR structures determined to date are of monomeric enzymes and this has been interpreted as a feature of this superfamily of proteins. A notable exception is the tetrameric K^+ Channel β subunit (AKR6A2) where the quaternary structure matches the 4-fold symmetry of the membrane-bound portion of the channel and more recently the dimeric xylose reductase of *Candida tenuis* (Wilson et al., this issue). There is strong evidence that the AKR7 enzymes are dimeric in solution and this is confirmed by the crystal structure of AKR7A1 (Fig. 2). The two subunits, which form the dimer, are related by almost perfect rotational 2-fold symmetry, each burying some 1000 $Å^2$ of solvent accessible surface area at the dimer interface. The interface involves almost exclusively helices α5 and α6 with eight hydrogen bonds and one salt bridge (between Lys-155 and Glu-118) contributed per subunit. The functional importance of the dimerisation of the AKR7 enzymes is not clear. The active sites of the two monomers are spatially arranged on opposite faces of the dimer. This means that the active sites are unlikely to interact with a membrane or other components of a transporter as is the case with AKR6A2. Loop C and the end of Helix H2 of the enzyme are involved in dimer interactions, which might suggest cooperative binding of substrate or co-factor; however, this has not been observed experimentally.

3.3. Active site features

The residues implicated in catalysis for other AKR are conserved in the active site of AKR7A1, namely Asp-40, Lys-73, Tyr-45, His-109. Tyr-45 and His109 together with the nicotinamide ring of NADP form an oxyanion binding site in which the aldehyde or ketone oxygen binds. Tyr-45 is most likely to act as the proton donor during catalysis as described for other AKR.

The main features of the AKR7A1 active site can be highlighted by comparing it to the active site of AKR1B1 (Fig. 3). Firstly the shape of the active site is very different due to the size and orientation of the various loop structures. In particular Loops A and C form a considerable part of the active site in AKR1 enzymes but both these loops are significantly shorter in AKR7A1,

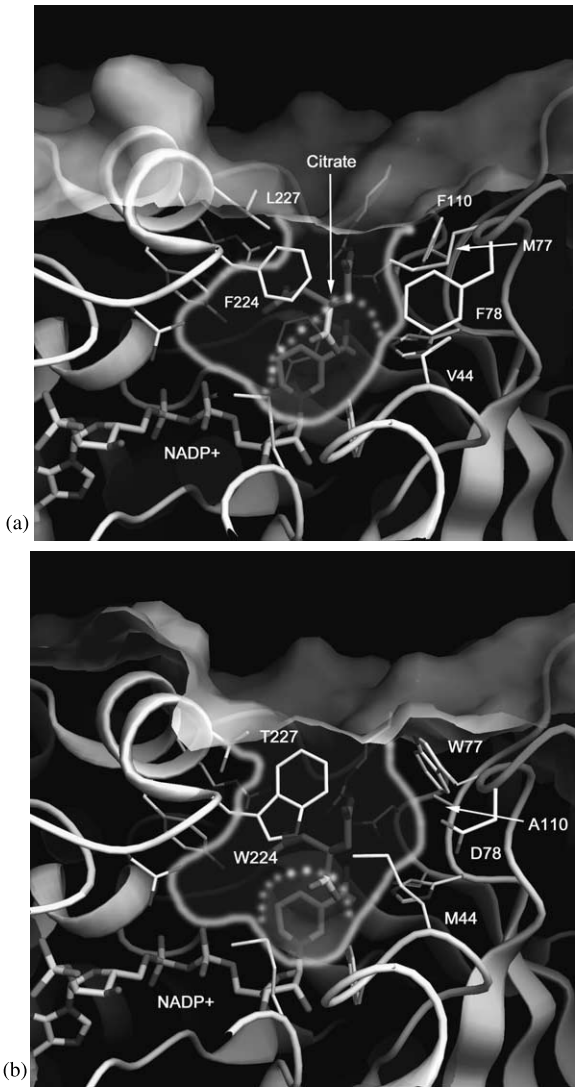

Fig. 5. A cross-section through a surface view of the active site of (a) AKR7A1 crystal structure (b) AKR7A4 molecular model. Both structures are shown in full and represented as ribbons with specific amino acids side chains labelled and shown in stick form. A solid airbrushed line represents the extent of the active site cavity, a dashed airbrush line the size of the opening to the solvent (exit). The positions of the cofactor $NADP^+$ and the inhibitor citrate inhibitor are shown in thicker stick. The surface calculated using GRASP [26] and the diagram was produced using DINO (http://www.biozentrum.unibas.ch/~xray/dino).

thus reducing the size of one side of the active site pocket. However, in AKR7 enzymes Loop B is significantly larger, therefore, building up the other side of the active site in comparison to AKR1B1. The net result of these differences is that AKR7A1 has a wide but shallow active site cavity ($11 \times 11 \times 7$ Å) compared with AKR1B1, which is narrower but deeper ($7 \times 12 \times 14$ Å). The loops of AKR7A1 almost completely close off the active site, in particular residues Met- 77 and Phe-78 from a short loop between strand β3 and α3 and residues Leu-227, and Phe-224 from Loop B are involved. These form a discrete entrance to and exit from the active site pocket for AKR7A1 that contrasts with that of AKR1B1 which is much more open.

The second significant feature of the AKR7A1 active site is that it has a strong positive charge due to three arginines residues Arg-17, Arg-231 and the extreme C-terminal Arg-327 that line the active site. AKR1B1 is more typical in having a predominantly non-polar surface to the active site (Fig. 3). In particular the guanidinium groups of Arg-231 and Arg-327 in AKR7A1 are 3.5 Å apart and perpendicular to each other forming a second potential anion-binding site, which is clearly of functional importance.

The differences in the active site pocket between AKR7A1 and AKR1B1 are highlighted in the mode of binding of the inhibitor citrate. In AKR1B1, citrate is bound in the active site solely by two hydrogen bonds to Tyr-48 and His-110 and van der Waals contacts to Val-47, Trp-111 and the cofactor $NADP^+$ (Fig. 3b). In AKR7A1, in addition to two hydrogen bonds formed by the catalytic residues (Tyr-45 and His-109) to citrate, hydrogen bonds also form to the second carboxylate of citrate and to the hydroxyl moiety via Tyr-228, Arg-231 and Arg-327. In so doing, one of the citrate carboxyl groups is buried within the active site in the region formed by Loop B, while the hydroxyl group of citrate forms hydrogen bonds with the carbonyl of $NADP^+$ and guanidinium group of Arg-327 (Fig. 3a). The burying of a second carboxylate of citrate in the active site of AKR7A1 provides a mechanism by which AKR7A1 can catalyse the reduction of 2-carboxy benzaldehyde, which would be sterically hindered in AKR1 enzymes. Reduction of aflatoxin dialdehyde to its dialcohol can also be explained by the availability of hydrogen bond doners in the active site to correctly orient the substrate and the reduced depth of the active site cavitity of AKR7A1 compared with other AKR1 enzymes which would sterically clash with the rest of the bulky aflatoxin molecule.

3.4. Modelling of AKR7A4 to understand substrate specificity differences between the rat AKR7 isoenzymes

A second enzyme, AKR7A4, is present in rat, which is 79% sequence identical to AKR7A1. Overall, the kinetic parameters and substrate specificities of rat AKR7A1 and AKR7A4 enzymes are similar [25]. Notable exceptions are SSA where there is a 20-fold difference in affinity (AKR7A1 K_m 163 μM and AKR7A4 K_m 6.4 μM) and 2-CBA where there is a 10-fold difference in affinity and a 2-fold difference in activity (AKR7A1 k_{cat} 82 min^{-1}, K_m 0.7 μM, and AKR7A4 k_{cat} 42 min^{-1}, K_m 10 μM). In an attempt to understand why these differences in affinity arise, modeling of AKR7A4 was carried out. One particular aim was to identify any structural support for the hypothesis that the main function of the enzyme is as a SSA reductase.

A sequence alignment of known sequences of the AKR7 family is shown in Fig. 4a next to the secondary structure calculated from the AKR7A1 crystal structure, highlighting the high level of sequence conservation for this AKR family. There are over sixty differences in sequence between AKR7A1 and AKR7A4, many are conservative changes, e.g. Arg-204 to Lys and Lys-206 to Arg. Of these differences in sequence only fifteen are found consistently between the two sub groups of AKR7 enzymes. Mapping the position of these fifteen changes in primary sequence onto the crystal structure of AKR7A1 (Fig. 4b) reveals that many are within the active site cavity, e.g. Val-44 to Met and Phe-110 to Ala. This suggests that there are structural differences between the two sub groups of enzyme and these should be reflected in differences in substrate specificites.

Analysis of the AKR7A4 model shows that the fold is identical and there are no unresolved steric clashes which would suggest gross conformational changes in the peptide chain. Indeed, the Ala-12 to Thr substitution results in a favourable hydrogen bond between the hydroxyl of the side chain and the side chain of Ser-50. In addition, the Ala-75 to Asn substitution allows an additional hydrogen bond with the side chain of Gln 90. The differences in the active site between the crystal structure of AKR7A1 and the homology model of AKR7A4 are shown in Fig. 5. The replacement of Met-77 by Trp and Phe-110 by Ala in the AKR7A4 model seems to be complimentary. The position occupied by the aromatic ring of Phe-110 in AKR7A1 structure, substituted by the side chain of Trp-77 at position 77 in the model.

Another significant difference is the substitution of Phe-224 (the amino acid which closes off the active site in AKR7A1) by Trp in the AKR7A4 model. This change represents a difference between AKR7A1 and the other AKR7 enzymes, which also have higher affinity for SSA. The AKR7A4 model predicts that the Val-44 to Met exchange would close the exit of the active site cavity. Overall, the combined changes of Met-77 to Trp, Phe-78 to Asp and Phe-110 to Ala, instead of confining the active site for a small substrate like SSA seem instead to widen it by more than an Angstrom.

Initially this result appeared discouraging. Undoubtedly the active site is modified in a discrete manner, but rather than restricting the active site and favouring the binding of a smaller charged substrate such as SSA, the model predicts that the AKR7A4 active site would be wider than that of AKR7A1. However, analysis of the changes between AKR7A1 and AKR7A4 further away from the active site suggests a mechanism by which the active site could in fact be more confined. Residue Tyr-232 plays a critical role in anchoring Loop B in AKR7A1, as the side chain hydroxyl forms hydrogen bonds to the invariant residues Asn-169 and Asn-194. The Tyr-232 to Phe switch is, therefore, significant as it suggests that the relative position of Loop B may be altered in AKR7A4. If this were the case, then a more favourable packing of residues 77 and 78 in the short loop between strand β3 and α3 and the residues at the end of Loop B would be possible, as these are different between AKR7A1 and AKR7A4. This would close up the active site and may, therefore, account for the differences seen in affinities for SSA.

4. Conclusions

The crystal structure of AKR7A1 provides a structural basis for understanding the substrate specificities of the AKR7 family enzymes as a whole. In particular, the discovery of a wide but relatively shallow active site with a strong positive electrostatic potential explains the enzyme family's preference for substrates such as 2-CBA and SSA. Modelling of the putative SSA reductase AKR7A4, shows that a specific region of the active site around the catalytic residues is modified, which should change the catalytic properties of the enzyme. However, the model of AKR7A4 provides no quick explanation for the differences in the enzyme's affinity for 2-CBA and SSA. Analysis of changes between AKR7A1 and the AKR7A4 model, further away from the active site suggest that Loop B may not adopt exactly the same conformation in AKR7A4 and together with hinged movements in the protein restrict the enzyme active site. The model predicts a number of amino acid residues that should be responsible for modifying substrate specificity. It is, however, not able to address whether the main function of isoenzymes such as AKR7A4 is as a SSA reductase.

Acknowledgements

We thank the members of Glasgow Protein Crystallography group for their help in this work, particularly Dr R. Thom for protein purification and B. Lohkamp for help with data collection. Funding from the BBSRC and Wellcome trust is also acknowledged, as is the support by 'European Community—Access to Research Infrastructure Action of the Improving Human Potential Programme' to the EMBL Hamburg Outstation, Contract Number HPRI-1999-00017.

References

[1] K. Bohren, B. Bullock, B. Wermuth, K. Gabbay, The aldo-keto reductase superfamily, J. Biol. Chem. 264 (1989) 9547–9551.

[2] J.M. Jez, T.G. Flynn, T.M. Penning, A new nomenclature for the aldo-keto reductase superfamily, Biochem. Pharmacol. 54 (1997) 639–647.

[3] J.M. Jez, T.M. Penning, The aldo-keto reductase (AKR) superfamily: an update, Chem.-Biol. Interact. 130 (2001) 499–525.

[4] J.M. Rondeau, F. Tete-Favier, A. Podjarny, J.M. Reymann, P. Barth, J.F. Biellman, D. Moras, Novel NADPH-binding domain revealed by the crystal structure of aldose reductase, Nature 355 (1992) 469–472.

[5] D.K. Wilson, K.M. Bohren, K.H. Gabbay, F.A. Quiocho, An unlikely sugar substrate site in the 1.65 Angstrom structure of the human aldose reductase holoenzyme implicated in diabetic complications, Science 257 (1992) 81–84.

[6] O. El-kabbani, K. Judge, S.L. Ginell, D.A.A. Myles, L.J. Delucas, T.G. Flynn, Structure of porcine aldehyde reductase holoenzyme, Nat. Struct. Biol. 2 (1995) 687–692.

[7] S.S. Hoog, J.E. Pawlowski, P.M. Alzari, T.M. Penning, M. Lewis, 3-Dimensional structure of rat-liver 3-alpha-hydroxysteroid dihydrodiol dehydrogenase—a member of the aldo-keto reductase superfamily, Proc. Natl. Acad. Sci. USA 91 (1994) 2517–2521.

[8] E. Hur, D.K. Wilson, The crystal structure of the GCY1 protein from S-cerevisiae suggests a divergent aldo-keto reductase catalytic mechanism, Chem.-Biol. Interact. 130 (2001) 527–536.

[9] S. Khurana, D.B. Powers, S. Anderson, M. Blaber, Crystal structure of 2,3-diketo-D-gluconic acid reductase A complexed with NADPH at 2.1-A resolution, Proc. Natl. Acad. Sci. USA 95 (1998) 6768–6773.

[10] J.M. Gulbis, S. Mann, R. MacKinnon, Structure of a voltage-dependent K+ channel beta subunit, Cell 97 (1999) 943–952.

[11] D.J. Judah, J.D. Hayes, J.C. Yang, L.Y. Lian, G.C.K. Roberts, P.B. Farmer, J.H. Lamb, G.E. Neal, A novel aldehyde reductase with activity towards a metabolite of aflatoxin B_1 is expressed in rat liver during carcinogenesis and following the administration of an antioxidant, Biochem. J. 292 (1993) 13–18.

[12] J.D. Hayes, D.J. Judah, G.E. Neal, Resistance to aflatoxin-B1 is associated with the expression of a novel aldo-keto reductase which has catalytic activity towards a cytotoxic aldehyde-containing metabolite of the toxin, Cancer Res. 53 (1993) 3887–3894.

[13] E.M. Ellis, D.J. Judah, G.E. Neal, J.D. Hayes, An ethoxyquin-inducible aldehyde reductase from rat liver that metabolizes aflatoxin B_1 defines a subfamily of aldo-keto reductases, Proc. Natl. Acad. Sci. USA 90 (1993) 10350–10354.

[14] E.M. Ellis, J.D. Hayes, Substrate specificity of an aflatoxin-metabolizing aldehyde reductase, Biochem. J. 312 (1995) 535–541.

[15] V.P. Kelly, L.S. Ireland, E.M. Ellis, J.D. Hayes, Purification from rat liver of a novel constitutively expressed member of the aldo-keto reductase 7 family that is widely distributed in extrahepatic tissues, Biochem. J. 348 (2000) 389–400.

[16] L.S. Ireland, D.J. Harrison, G.E. Neal, J.D. Hayes, Molecular cloning, expression and catalytic activity of a human AKR7 member of the aldo-keto reductase superfamily: evidence that the major 2-carboxybenzaldehyde reductase from human liver is a homologue of rat aflatoxin B_1 aldehyde reductase, Biochem. J. 332 (1998) 21–34.

[17] L.P. Knight, E.A. Primiano, J.D. Groopman, T.W. Kensler, T. Sutter, cDNA cloning, expression and activity of a second human aflatoxin B_1-metabolising member of the aldo-keto reductase superfamily, AKR7A3, Carcinogenesis 7 (1999) 1215–1223.

[18] A. Hinshelwood, G. McGarvie, E. Ellis, Characterisation of a novel mouse liver aldo-keto reductase AKR7A5, FEBS Lett. 523 (2002) 213–218.

[19] M. Schaller, M. Schaffhauser, N. Sans, B. Wermuth, Cloning and expression of succinic semialdehyde reductase from human brain—Identity with aflatoxin B-1 aldehyde reductase, Eur. J. Biochem. 265 (1999) 1056–1060.

[20] E. Kozma, E. Brown, E.M. Ellis, A.J. Lapthorn, The crystal structure of rat liver AKR7A1—A dimeric member of the aldo-keto reductase superfamily, J. Biol. Chem. 277 (2002) 16285–16293.

[21] J.M. Gulbis, M. Zhou, S. Mann, R. MacKinnon, Structure of the cytoplasmic beta subunit—T1 assembly of voltage dependent K+ channels, Science 289 (2000) 123–127.

[22] A. Perrakis, R. Morris, V.S. Lamzin, Automated protein model building combined with iterative structure refinement, Nat. Struct. Biol. 6 (1999) 458–463.

[23] G.N. Murshudov, A.A. Vagin, E.J. Dodson, Refinement of macromolecular structures by the maximum-likelihood method, Acta Crystallogr. Sect. D 53 (1997) 240–255.

[24] K.L. Kavanagh, M. Klimacek, B. Nidetzky, D.K. Wilson, The structure of apo and holo forms of xylose reductase, a dimeric aldo-keto reductase from Candida tenuis, Biochemistry 41 (2002) 8785–8795.

[25] V.P. Kelly, P.J. Sherratt, D.H. Crouch, J.D. Hayes, Novel homodimeric and heterodimeric rat gamma-hydroxybutyrate synthases that associate with the Golgi apparatus define a distinct subclass of aldo-keto reductase 7 family proteins, Biochem. J. 366 (2002) 847–861.

[26] A. Nicholls, K.A. Sharp, B. Honig, Protein folding and association—insights from the interfacial and thermodynamic properties of hydrocarbons, Proteins 11 (1991) 281–296.

[27] P. Gouet, E. Courcelle, D.I. Stuart, F. Metoz, ESPript: multiple sequence alignments in PostScript, Bioinformatics 15 (1999) 305–308.